Tunable Sub-wavelength Acoustic Energy Harvesting with Metamaterial Plate

Mourad Oudich, Yong Li

▶ **To cite this version:**

Mourad Oudich, Yong Li. Tunable Sub-wavelength Acoustic Energy Harvesting with Metamaterial Plate. Journal of Physics D: Applied Physics, 2017, 50 (31), pp.315104. ⟨10.1088/1361-6463/aa779d⟩. ⟨hal-04981040⟩

HAL Id: hal-04981040

https://hal.science/hal-04981040v1

Submitted on 6 Mar 2025

HAL is a multi-disciplinary open access archive for the deposit and dissemination of scientific research documents, whether they are published or not. The documents may come from teaching and research institutions in France or abroad, or from public or private research centers.

L'archive ouverte pluridisciplinaire **HAL**, est destinée au dépôt et à la diffusion de documents scientifiques de niveau recherche, publiés ou non, émanant des établissements d'enseignement et de recherche français ou étrangers, des laboratoires publics ou privés.

HAL Authorization

Tunable Sub-wavelength Acoustic Energy Harvesting with Metamaterial Plate

Mourad Oudich[1,2]**, and Yong Li**[3,4]

[1]CNRS, Institut Jean Lamour, Vandœuvre-lès-Nancy F-54500, France
[2]Université de Lorraine, Institut Jean Lamour, Boulevard des Aiguillettes, BP: 70239, Vandœuvre-lès-Nancy 54506, France
[3]Institute of Acoustics, School of Physics Science and Engineering, Tongji University, Shanghai 200092, P. R. China
[4]Shanghai Key Laboratory of Special Artificial Microstructure Materials and Technology, School of Physics Science and Engineering, Tongji University, Shanghai 200092, P. R. China

E-mail: mourad.oudich@univ-lorraine.fr, yongli@tongji.edu.cn

Abstract. We report theoretically on a sub-wavelength acoustic energy harvesting (AEH) using a thin acoustic metamaterial (AM) made of spring-mass resonators attached to the surface of a homogeneous elastic thin plate. Considering an incident acoustic wave hitting the AM plate, tunable and high efficient AEH is achieved by introducing a sub-wavelength defect inside the AM structure to confine the elastic energy into a spot which is then electromechanically converted into electrical power using a ceramic PZT patch. Several types of sub-wavelength cavities capable of confining acoustic energy at the sonic regime are extensively investigated for the optimization of AEH. Three analytical approaches, band structure, sound transmission loss and electrical-to-mechanical energy conversion, are proposed to fully describe the system interaction with the acoustic wave and quantify the AEH performance. Computed results show that an average power of 18 μW can be harvested using a specific cavity design of only 3×3 cm^2 size from an incident acoustic wave with a sound pressure level of 100 dB at 520 Hz. Such system can open a way through the design of effective tunable sub-wavelength acoustic energy harvesters based on AM applied to scavenge energy from sound.

Keywords: acoustic energy harvesting, acoustic metamaterial, piezoelectric effect

1. Introduction

Nowadays, sensors and actuators oil the wheels of our daily life and change our life style. We are witnessing an incredible development of sensing technologies motivated by the increasing demand and the industrial competition. Powering these devices is of essence and it is mostly done by mean of batteries which struggle to follow up the sensors development. In fact, not only electrical batteries are cumbersome and constrain miniaturization, but their power supply is limited and have a short lifetime relative to sensors. Meanwhile, one of the advantages of MEMS based sensors is their low energy consumption as their operating power is less than 100 μW for a device size less than 1 cm^3. Thus, it is essential to continuously adapt the power supply to the micro-devices which are permanently active, as batteries are to be frequently recharged, replaced and cleared out, not to mention the environmental chemical risks. It becomes now vital to promote other electrical powering technologies and the most attractive solution is energy harvesting. There are numerous sources providing available and free energy in our environment, either electromagnetic, thermal, mechanical or biochemical. Scientific researchers work actively to come up with new efficient technologies to exploit these sustainable but permanently lost energies.

In the last decade, there has been active research on harvesting energy from ambient vibrations using direct piezoelectric (PE) effect [1, 2, 3, 4]. PE materials are now a key for mechanical-to-electrical energy conversion as they perform good electro-mechanical coupling mechanism. Many works have been devoted to come up with solutions for acoustic energy harvesting (AEH) in the sonic frequency range from the sound pressure level (SPL) of discomfort to the loudest possible threshold (194 dB). The earliest works used acoustic energy harvesters based on Helmholtz resonator. Hotowitz et al [1] proposed a micro-scale energy harvester composed of a Helmholtz resonator where the small aperture or neck is connected to the environment and the back wall of the cavity is made of a flexural diaphragm. They attached a PE ring into the diaphragm and connected it electrically into a load resistor for the purpose of electrical impedance matching. At the Helmholtz resonance frequency, the high amplitude of the diaphragms mechanical vibration induces strain into the PE ring which generates electrical voltage by direct PE effect. A maximum output power density of 100 μW.cm^{-2} was obtained at the resonant frequency for 980 Ω load resistance and 149 dB of the acoustic pressure. In another work, Noh et al [2] combined a Helmholtz resonator and a PE cantilever to perform AEH. The high sound acoustic pressure inside the resonant cavity causes the composite PE cantilever to vibrate and produce electrical power. A maximum power of 0.1 μW was reached at 860 Hz. Another approach was proposed by Li et al [3, 4] who placed an array of PE beam inside a long tube Helmholtz resonator in order to increase the efficiency of the AEH. By testing multiple configurations regarding the PE beam number and spacing, they were able to obtain, both theoretically and experimentally, a maximum output power of approximately 0.31 mW collected by 4 PE beams at 190 Hz from 100 dB of SPL inside a 20 m tube.

As an alternative to Helmholtz resonators approach, sonic crystals (SC) were introduced in some few works to perform acoustic energy confinement for the purpose of AEH. SC is a

periodic composite structure which has the ability of creating band gaps where acoustic wave propagation is prohibited [5, 6, 7, 8]. This property opened the way to perform acoustic wave manipulation: confinement and wave-guiding for instance. In fact, by creating a point or a line defect inside the SC, acoustic modes can be created at frequencies inside the band gap and the acoustic wave can be trapped inside the defect or along the waveguide [9, 10, 11]. In 2009, Wu et al [12] proposed an acoustic energy harvester based on a SC made of cylindrical rods in air with 4.9 cm period, in which they created a point defect by removing a single rod. An acoustic confined cavity mode is created inside the defect at 4.02 kHz in the band gap. By placing a piezoelectric PVDF film inside the defect, they were able to get a maximum power output of approximately 35 nW generated by an acoustic wave with a SPL of 80 $\sim$ 100 dB [13]. Recently, Yang et al [14] presented an enhancement of AEH by placing an electromechanical Helmholtz resonator inside a SC defect center. By combining the coupled Helmholtz and cavity resonances, they were able to generate 429 μW of maximum power with an optimal load resonance of 4.4 kΩ for an incident acoustic wave pressure of 110 dB. In all these works, the size of the sonic crystal super-cell is at least 17$\times$17 cm^2 and the rods length is of 10 cm, which constraints the objective of small size AEH. This limitation is due to the large acoustic wavelength at the sonic frequency range, as the band gap creation is based on the Bragg scattering mechanism. The crystals lattice constant is constrained as it is to be in the same order as the targeted acoustic wavelength. To overcome this limitation, Liu et al [15] introduced the concept of acoustic metamaterial (AM) capable of band gap creation at wavelengths much larger than periodicity of the system [16, 17]. The band gap opening is based on local resonance mechanism and becomes independent of the periodicity of the structure. AM are composite structures capable of demonstrating unusual physical properties for acoustic and elastic waves [17, 18, 19, 20, 21, 22, 23, 24, 25, 26, 27, 28, 29, 30, 31]. One of these properties is the possibility to perform divergent and even negative effective mass density for acoustic waves by considering the homogenization approach at wavelengths higher than the AM structuration. The infinite behavior of the effective mass density paved the way through the design of artificial systems capable of breaking the mass density law limitation and achieving low frequency sound mitigation with smile size structure compared to the wavelength [16, 32, 33, 34, 35]. Regarding AEH application, Ma et al [33] proposed a membrane-type system composed of a decorated membrane and a back cavity. The incident energy around 152 Hz is totally absorbed by creating the resonant state of the system with deep-subwavelength thickness of 17 mm. By employing magnet wires carried by the membrane and four pairs of neodymium magnets along the magnet wires, high acoustic-electric energy conversion efficiency of 23% is realized by the up-and-down oscillation of the membrane. Recently, we have proposed an AM plate made of periodic distribution of rubber pillars over an aluminum plate of thickness 0.5 mm, where the lattice constant is 1 cm [23]. The AEH approach was performed using a cavity created inside the AM plate by removing 4 pillars and a PE thin cylindrical layer was attached to the plate in the cavity. Considering the airborne sound configuration, we have demonstrated theoretically the possibility of harvesting a maximum power of 8.8 μW at 2257 Hz from 100 dB SPL with only 6$\times$6 cm^2 for the surface size area and 5.5 mm for the total AM plate system thickness. However, for such

system, the cavity size remains constraining if one is looking for the same cavity mode at lower frequencies where the wavelength is larger than the cavity size. It is therefore highly desired to achieve a tunable AEH at low frequency with high efficiency, which is not realized by previous works.

In this study we will introduce a different method to create a cavity mode with small size (less than 3 cm) inside an AM plate. This method overcomes the cavity size limitation and allows us to perform AEH at frequency range around 500 Hz where the wavelength in air is about 70 cm and at least 10 cm in the bare aluminum plate. An efficient analytical approach is presented in this paper to perform the band structures, transmission loss of the proposed AM plates and estimate the amount of power harvested from acoustic incident wave. Tunable AEH is successfully realized in low frequency range with subwavelength cavity size, providing a feasible way to harvest low frequency acoustic energy. The paper is organized as follows: in section II, we introduce the AM plate system considered for the analytical model and present the acoustical, the mechanical and the electrical formulas for the calculation of the sound transmission loss, the band structure and the harvested electrical power. In section III, we apply the model to two kinds of cavity systems and discuss the obtained results.

2. Metamaterial plate system for energy harvesting

The simplified model considered for the metamaterial system is a thin infinite plate in which the surface is decorated with a square array of spring mass resonators as shown in figure 1(a). This representation is one of the simplest and most used models for analytical studies regarding AM plates. The figure presents the system in the airborne sound configuration where the incident sound wave comes from the air region denoted Air1 and hits the plate surface. The amount of the sound pressure transmitted through the plate into the air region denoted Air2 gives the sound transmission loss (STL). The periodicity of the AM structure and the plate thickness are denoted a and e respectively, which are fixed in the whole study into 1 cm and 0.5 mm respectively. The incident SPL is considered to be at 100 dB which corresponds to 2 Pa for the pressure amplitude.

Based on the Kirchhoff plate theory, Xiao et al [35] presented an analytical model for the band structure and STL calculation for any kind of periodic distribution of spring mass resonators over a thin plate. Their model can be used for supercell systems containing different geometrical defect structures. We apply the model to study the confinement of the elastic waves inside a cavity in the AM plate in the airborne sound configuration. The cavity is designed to create a defect mode within the band gap where acoustic energy can be confined into a spot inside the structure (figure 1(b)). Circular PE patch device can be then used to convert the mechanical vibration into electrical power. The purpose of this study is to evaluate how much acoustic energy can be harvested using a confined cavity mode inside the metamaterial system.

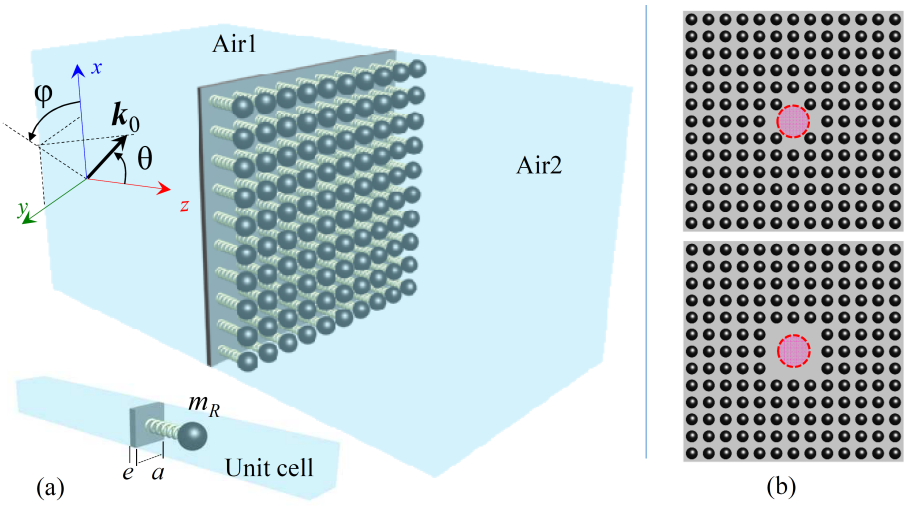

Figure 1. (a) Metamaterial structure in the airborne sound configuration and the unit cell associated to the system. The inset represents the unit cell of the structure (b) Examples of Supercells where the cavity is created by removing several resonators. The red circle presents the PE patch placement for AEH.

2.1. Band structure calculation

The band structure calculation is essential to understand the mechanical vibrational motion of the elastic plate system when it interacts with the sound wave coming from air [36]. For the analytical band structure calculation, we start from the governing equation of wave propagation in the plate, based on the Kirchhoff plate theory:

$$D\nabla^4 w(\mathbf{r}) - \rho h\omega^2 w(\mathbf{r}) = \sum_{j=1}^{N}\sum_{\mathbf{R}} f_j(\mathbf{r}_j+\mathbf{R})\,\delta\left[\mathbf{r}-(\mathbf{r}_j+\mathbf{R})\right], \tag{1}$$

where $w(\mathbf{r})$ is the transverse displacement field of the plate, $\mathbf{r}=(x,y)$ is the in-plan position in the plate and $D=Eh^3/12(1-\nu^2)$ is the plate bending stiffness, E, ν and ρ are the Youngs modulus, Poissons ratio and mass density of the plate material respectively. As we assume that we have N resonators distributed in the surface of the plate, f_j is the force applied to the plate by the resonator located at $\mathbf{r}_j+\mathbf{R}$ where $\mathbf{r}_j=(x_j,y_j)$ represents the location of the jth resonator in the supercell depicted in figure 1, and $\mathbf{R}=(ma_N,na_N)$ where m and n are integers and $a_N=Na$ is the super-lattice constant of the square periodic structure. Due to the periodicity of the system, the transverse displacement $w(\mathbf{r})$ can be written as:

$$w(\mathbf{r}) = \sum_{\mathbf{G}} w_{\mathbf{G}} e^{-i(\mathbf{k}+\mathbf{G}).\mathbf{r}}, \tag{2}$$

where the $\mathbf{G}=2\pi(m',n')/a_N$ is the reciprocal super-lattice vector, and $k=(k_x,k_y)$ the wave vector. In another hand, we have also:

$$f_j(\mathbf{r}_j+\mathbf{R}) = f_j(\mathbf{r}_j)\,e^{-i\mathbf{k}.\mathbf{R}}. \tag{3}$$

Then, one can obtain:

$$\sum_{\mathbf{R}} f_j\left(\mathbf{r}_j+\mathbf{R}\right)\delta\left[\mathbf{r}-\left(\mathbf{r}_j+\mathbf{R}\right)\right]=f_j\left(\mathbf{r}_j\right)e^{-i\mathbf{k}.\left(\mathbf{r}-\mathbf{r}_j\right)}\sum_{\mathbf{R}}\delta\left[\mathbf{r}-\left(\mathbf{r}_j+\mathbf{R}\right)\right]. \tag{4}$$

Furthermore, one can write:

$$\sum_{\mathbf{R}}\delta\left[\mathbf{r}-\left(\mathbf{r}_j+\mathbf{R}\right)\right]=\sum_{\mathbf{G}}\frac{1}{S}e^{-i\mathbf{G}.\left(\mathbf{r}-\mathbf{r}_j\right)}, \tag{5}$$

where $S=a_N^2$ is the surface of the super-cell. Then from equations (4) and (5):

$$\sum_{\mathbf{R}} f_j\left(\mathbf{r}_j+\mathbf{R}\right)\delta\left[\mathbf{r}-\left(\mathbf{r}_j+\mathbf{R}\right)\right]=f_j\left(\mathbf{r}_j\right)e^{-i\mathbf{k}.\left(\mathbf{r}-\mathbf{r}_j\right)}\sum_{\mathbf{G}}\frac{1}{S}e^{-i\mathbf{G}.\left(\mathbf{r}-\mathbf{r}_j\right)}. \tag{6}$$

Regarding the force applied by each resonator in the super-cell, we have:

$$f_j\left(\mathbf{r}_j\right)=-K_j\left(u_j-w\left(\mathbf{r}_j\right)\right)=-\omega^2 m_j u_j, \tag{7}$$

where u_j is the displacement of the resonators mass and K_j and m_j are the stiffness and the mass of the spring-mass resonator located in position $\mathbf{r}_j$. By inserting equations (2) and (6) into equations (1) and (7), one can come up with the following equations:

$$\begin{aligned} SD\left[(k_x+G_x)^2+(k_y+G_y)^2\right]^2 w_{\mathbf{G}}+\sum_{j=1}^{N}K_j\left(\sum_{\mathbf{G}'}w_{\mathbf{G}'}e^{-i(\mathbf{k}+\mathbf{G}')\mathbf{r}_j}-u_j\right)e^{i(\mathbf{k}+\mathbf{G})\mathbf{r}_j} \\ =S\rho h\omega^2 w_{\mathbf{G}}, \\ -K_j\left(\sum_{\mathbf{G}'}w_{\mathbf{G}'}e^{-i(\mathbf{k}+\mathbf{G}')\mathbf{r}_j}-u_j\right)=m_j\omega^2 u_j. \end{aligned} \tag{8}$$

From equations (8) one can construct an eigenvalue problem to calculate the eigenfrequencies and get the band structure of the AM plate system.

2.2. STL calculation

For the STL calculation, we assume an incident plane wave pressure P_i in air region Air1 hitting the plate with an elevation and azimuth angles θ and φ respectively (figure 1(a)). If the waves pressure amplitude is denoted P_0, then,

$$P_i\left(\mathbf{r},z\right)=P_0 e^{-i(\mathbf{k_r}.\mathbf{r}+k_z z)}, \tag{9}$$

where $\mathbf{k_r}=(k_x,k_y)$, $k_x=k_0\sin\theta\cos\phi$, $k_y=k_0\sin\theta\sin\phi$, $k_z=k_0\cos\theta$and $k_0=\omega/c_0$. c_0 is the sound velocity in air.Based on the Kirchhoff plate theory, we start from the governing equations of wave propagation in thin plate in the airborne sound configuration by considering the plate along the XY plane located in position $z=0$ and considering the air wave pressures:

$$\begin{aligned} D\nabla^4 w\left(\mathbf{r}\right)-\rho h\omega^2 w\left(\mathbf{r}\right)= \; & p_i(\mathbf{r},z)_{z=0}+p_{ref}(\mathbf{r},z)_{z=0}-p_{tr}(\mathbf{r},z)_{z=0} \\ & +\sum_{j=1}^{N}\sum_{\mathbf{R}}f_j\left(\mathbf{r}_j+\mathbf{R}\right)\delta\left[\mathbf{r}-\left(\mathbf{r}_j+\mathbf{R}\right)\right], \end{aligned} \tag{10}$$

where $p_m(\mathbf{r},z)_{z=0}$ with $m = i,ref,tr$ are the incident, reflected and transmitted waves respectively. Using the plane wave expansion, the reflected and the transmitted sound pressures can be expressed as:

$$\begin{aligned} P_{ref} &= \sum_{\mathbf{G}} P_{ref,\mathbf{G}} e^{-i(\mathbf{k_r}+\mathbf{G}).\mathbf{r}+ik_{z,\mathbf{G}}z}, \\ P_{tr} &= \sum_{\mathbf{G}} P_{tr,\mathbf{G}} e^{-i(\mathbf{k_r}+\mathbf{G}).\mathbf{r}-ik_{z,\mathbf{G}}z}, \end{aligned} \tag{11}$$

where

$$k_{z,\mathbf{G}} = \begin{cases} \sqrt{k_0^2 - |\mathbf{k_r}+\mathbf{G}|^2} & k_0^2 \geq |\mathbf{k_r}+\mathbf{G}|^2 \\ -i\sqrt{|\mathbf{k_r}+\mathbf{G}|^2 - k_0^2} & k_0^2 < |\mathbf{k_r}+\mathbf{G}|^2 \end{cases}. \tag{12}$$

Meanwhile, from equation (7), one can deduce the relationship between $f_j\left(\mathbf{r}_j\right)$ and $w\left(\mathbf{r}_j\right)$ for each resonator j:

$$f_j\left(\mathbf{r}_j\right) = -D_j w\left(\mathbf{r}_j\right) \tag{13}$$

where

$$D_j = \frac{-\omega^2 m_j}{1 - \omega^2 \Big/ \omega_j^2(1+i\eta_j)}, \tag{14}$$

$\omega_j = \sqrt{K_j/m_j}$ and η_j are respectively the angular resonance frequency and the loss factor for the spring-mass resonator j. To calculate the unknown reflected and transmitted pressure as well as the displacement field of the plate, the boundary conditions are expressed in the air-plate contact interfaces. Thus, the boundary conditions expressing the normal velocity continuity at the air-plate interface are:

$$\begin{aligned} \left.\frac{\partial\left(p_i(\mathbf{r},z)+p_{ref}(\mathbf{r},z)\right)}{\partial t}\right|_{z=0} &= \rho_0\omega^2 w\left(\mathbf{r}\right), \\ \left.\frac{\partial p_{tr}(\mathbf{r},z)}{\partial t}\right|_{z=0} &= \rho_0\omega^2 w\left(\mathbf{r}\right). \end{aligned} \tag{15}$$

By inserting equations (2) and (11) into equations (15), and considering that the sum is for any possible $\mathbf{r}$, we can drive two relationships between the sound pressures and the plate displacement coefficients:

$$\begin{aligned} p_{ref,\mathbf{G}} &= P_0\delta_{\mathbf{G}-\mathbf{0}} - \frac{i\rho_0\omega^2}{k_{z,\mathbf{G}}} w_{\mathbf{G}}, \\ p_{tr,\mathbf{G}} &= \frac{i\rho_0\omega^2}{k_{z,\mathbf{G}}} w_{\mathbf{G}}. \end{aligned} \tag{16}$$

Furthermore, substituting equations (2), (6), (9), (11) and (13) into equation (10), one can have a third relationship:

$$\begin{aligned} &\left\{ SD\left[(k_x+G_x)^2 + (k_y+G_y)^2\right]^2 + \omega^2\left[2\rho_0 i/k_{z,\mathbf{G}} - \rho e\right] S \right\} w_{\mathbf{G}} \\ &+ \sum_{j=1}^{N} D_j \left(\sum_{\mathbf{G}'} w_{\mathbf{G}'} e^{-i(\mathbf{G}'-\mathbf{G})\mathbf{r}_j} \right) = 2P_0 S\delta_{\mathbf{G}-\mathbf{0}} \end{aligned} \tag{17}$$

By choosing finite number of reciprocal lattice, one can use the linear equations (16) and (17) to get the plane waves components $w_{\mathbf{G}}$, $p_{ref,\mathbf{G}}$ and $p_{tr,\mathbf{G}}$. Then, using equation (11), the transmitted sound pressure can be calculated and used to calculate the STL:

$$\mathrm{STL(dB)} = 20\log_{10}\left(|P_{tr}/P_i|\right). \tag{18}$$

2.3. Electrical model

We consider a ceramic PE PZT thin cylindrical transducer patch attached into the plate surface empty of resonators. The PZT is placed at the center of the cavity as it is indicated by red circle in figure 1(b). In this whole study, the thickness of the PZT layer is fixed to 0.1 mm. In our approximation, we consider that the effect of the piezo-mechanical coupling on the cavity mode shape and its frequency is neglected. Based on the elastic theory of thin beams, the strain along x and y direction are:

$$S_x = -z\frac{\partial^2 w}{\partial x^2};\ S_y = -z\frac{\partial^2 w}{\partial y^2};\ \text{and}\ S_{xy} = -z\frac{\partial^2 w}{\partial x \partial y}. \tag{19}$$

We assume that the PZT thin layer added to the surface does not change the deformed shape of the mode and only increases the equivalent bending stiffness of the plate. Consequently, the amplitude of the vibration under the same excitation is slightly reduced in comparison to the same system without the PZT. The linear PE theory is used in this study. As the PE layer thickness is very small compared to the plate dimensions, we assume that the stress in z direction within the PZT equals to zero. Consequently, the electrical displacement along x and y directions are: $D_x = D_y = 0$. The electrical displacement along the z-direction within the PZT is expressed as function of the strain in the x and y directions and the electric field:

$$D_z = \varepsilon_{33} E_z + e_{31} S_x + e_{32} S_y + e_{36} S_{xy}, \tag{20}$$

where $(e_{3m})_{m=1,2,6}$ are the PE constants along the $3m$ coupling direction, ε_{33} is the dielectric permittivity along the third direction and E_z is the electric field along the z direction within the PZT layer. In this study we consider that $e_{31} = e_{32} = -6.62281$ C/m^2, $e_{36} = 0$ and $\varepsilon_{33} = 1433.6\varepsilon_0$.

Let us assume that the PZT face in contact with the plate is connected to the ground and the other free surface is covered by an electrode layer which is connected to a resistor to form a closed electrical circuit. In this way, the electrical potential on the PZT surface is the same. The charge Q collected on the electrode surface can be expressed as:

$$Q = \int_{\mathrm{A}} D_z \mathrm{dA} = \int_{\mathrm{A}} \left(\varepsilon_{33} E_z + e_{31} S_x + e_{32} S_y\right) \mathrm{dA}, \tag{21}$$

where the integral is over the electrode surface denoted A of the PZT layer. Assuming that the electrical potential between the PZT surfaces having normal z-direction is denoted V, under the uniform electrical field assumption, the electrical voltage can be approximately expressed as:

$$V \approx -t_{\mathrm{PZT}} E_z, \tag{22}$$

where t_{PZT} is the thickness of the PZT layer. From equations (19), (21) and (22), one can have the following expression for the collected charge:

$$Q = \Phi - \pi r_{PZT}^2 \frac{V}{t_{PZT}}, \tag{23}$$

where r_{PZT} is the radius of the PZT patch and Φ has the following expression:

$$\Phi = -\frac{e}{2}\int_{\mathrm{A}}\left(e_{31}\frac{\partial^2 w}{\partial x^2}+e_{32}\frac{\partial^2 w}{\partial y^2}\right)\mathrm{dA}. \tag{24}$$

Using the PWE decomposition (equation (2)) for the out-of-plane displacement, one can evaluate Φ as

$$\Phi = \frac{e}{2}\sum_{\mathbf{G}}\left[e_{31}\left(\mathbf{k}+\mathbf{G}\right)_x^2+e_{32}\left(\mathbf{k}+\mathbf{G}\right)_y^2\right]w_{\mathbf{G}}\int_{\mathrm{A}} e^{-i(\mathbf{k}+\mathbf{G}).\mathbf{r}}\mathrm{dA}. \tag{25}$$

The current, the charge and the voltage are dependent upon the mechanical vibrations. The relationship between the current amplitude and that of the charge is

$$I = \omega Q. \tag{26}$$

For the electrical circuit with pure resistance denoted R, we have also the relationship between the voltage and the current

$$I = \frac{V}{R} \tag{27}$$

The voltage has the same phase as the current. Combining equations (23), (26) and (27), one can have the following expression for the amplitude of the current

$$I = \frac{\omega\Phi}{\left(1+\omega\varepsilon_{33}R\frac{\pi r_{\mathrm{PZT}}^2}{t_{\mathrm{PZT}}}\right)}. \tag{28}$$

For the AC electrical circuit, the time average of the output power is as below,

$$\bar{P} = \frac{V}{\sqrt{2}}\frac{I}{\sqrt{2}} = R\frac{I^2}{2} = \frac{R\omega^2\Phi^2}{2\left(1+\omega\varepsilon_{33}R\frac{\pi r_{\mathrm{PZT}}^2}{t_{\mathrm{PZT}}}\right)^2}. \tag{29}$$

Using this expression, one can estimate the collected power as function of the load resistance and the PZT surface geometry. Despite its efficiency for theoretical studies regarding realistic structures, FEM as we employed in [23] is time consuming especially for bigger size systems with small size structuration. Analytical formulation for the same problem, whenever it is possible using approximation technics, can give good results in a very short time.

Throughout the calculations, the material parameters of the AM plate are $E = 70\mathrm{E}9$ Pa, $\nu = 0.33$, and $\rho = 2700$ kg/m^3, where E, ν and ρ represent the Young's Modulus, poison's ratio and density. The density and velocity used for air is 1.21 kg/m^3 and 343 m/s. The effect of the resonators is treated as an effective force on the AM plate.

3. Results and Discussions

3.1. Empty defect system

In this section, we apply the model to a square supercell made of 11x11 unit cells in which we remove a specific number of unit resonators to create a cavity defect mode. Our study holds for two systems: the first structure is presented in figure 2(a) where the central resonator

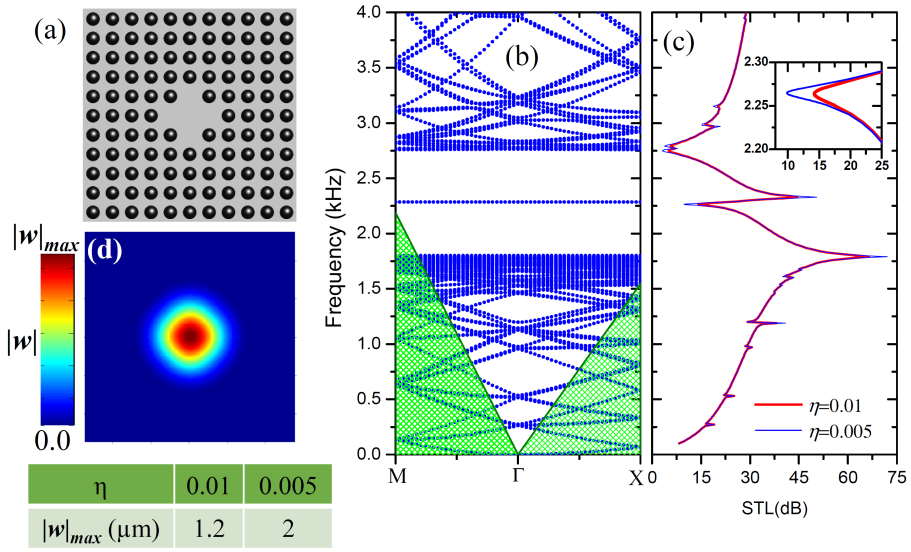

η	0.01	0.005
$\|w\|_{max}$ (μm)	1.2	2

Figure 2. (a) Supercell of the AM Plate structure where the defect is created by removing the five central resonators. (b) The band structure calculation for the supercell. (c) STL for loss factor $\eta = 0.01$ (red solid bold line) and $\eta = 0.005$ (blue solid line). The inset is a zoom in the STL dip around 2.25 kHz. (d) The displacement field of the plate at the cavity mode frequency. The table is the maximum value of the displacement for field for $\eta = 0.01$and $\eta = 0.005$.

was removed as well as the first closest resonators to the center: a total of five resonators are removed.

Figure 2(b) presents the band structure calculation for the periodic super-cell system in both ΓX and ΓM directions of the first Brillouin zone. The sound line is plotted in green color in both directions and the shaded region under this line indicates the modes that cannot be excited by the incident acoustic wave in the airborne sound configuration [36]. From figure 2(b), one can easily deduce the band gap region where a flat mode exists which corresponds to the cavity mode located at approximately 2285 Hz. In this case the mass of the resonators is 184 μg and the resonance frequency is fixed to be 1.8 kHz. These properties will allow the creation of a band gap between 1.8kHz and 2.76 kHz for flexural waves. The resonators mechanical properties were chosen so that the frequency of the created cavity mode will be localized in the middle of the band gap, which will increase the elastic energy confinement inside the defect space.

We plot in figure 2(c) the STL we can get by the supercell for an acoustic wave with normal incidence. The calculations were performed for two values of the loss factor η considered for the resonators: 0.01 and 0.005, plotted in bold red line and thin blue line respectively. From the STL figure, we find that at least 70 dB can be generated at the resonance frequency 1.8 kHz using the AM plate if we consider the sound mitigation purpose [36]. Furthermore, one can point out the dip at 2285 Hz located exactly at the cavity modes frequency. At this frequency, we plotted in figure 2(d) the norm of the out-of-plane

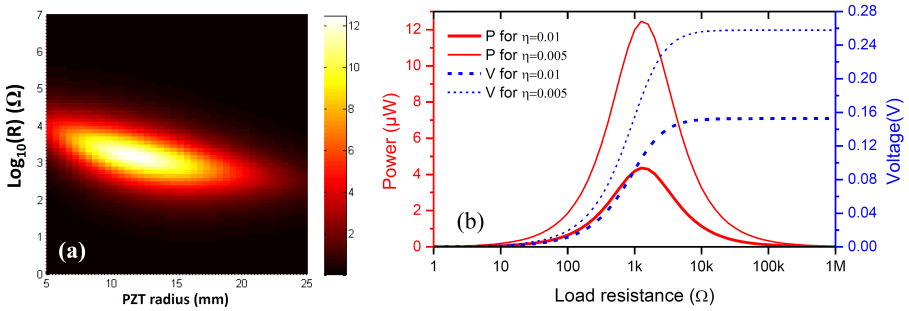

Loss factor η	0.01	0.005
Maximum power (μW)	4.35	12.46
PZT Radius (mm)	11.5	
Load Resistance (Ω)	1258.9	

Figure 3.) Output average power in color map as function of the PZT radius and the load resistance for $\eta = 0.005$ at the cavity mode frequency 2285 Hz. (b) Out-put power (solid lines) and voltage (dashed lines) for PZT radius 11.5 mm performed for both $\eta = 0.01$ and $\eta = 0.005$. The table summarizes the maximum power harvested with the optimal PZT radius and load resistance.

displacement w in the plate to get the cavity mode shape. We can deduce the elastic wave confinement within the defect space created inside the AM plate. Meanwhile, in figure 2(c), the STL dip matching the cavity mode corresponds to high transmission of the acoustic wave through the AM plate supercell as the cavity mode plays the role of a point source emitting an acoustic wave into the Air2 region. The STL of the dip is found to be at 9.84 dB for $\eta = 0.005$ and 14.24 dB for $\eta = 0.01$ (see inset in figure 2(c)). This can be easily understood as for high η values, an amount of the elastic energy in the plate is lost by the viscoelastic effect in the resonators and the amplitude of the cavity modes out-of-plane vibration becomes smaller in the case of $\eta = 0.01$ compared to the case $\eta = 0.005$ (see table in figure 2).

For AEH application, we used equation (29) to estimate the average power that can be scavenged from the system using a PZT circular patch placed in the center of the defect in the plate surface without resonators. From the expression, one can see that the power depends on the load resistance and the PZT radius. It is important to look for the optimized resistance for the purpose of electrical impedance matching as well as the optimized PZT radius for maximum power output.

In figure 3(a), we plot the output average power in color map as function of the PZT radius and the load resistance for $\eta = 0.005$ at the cavity mode frequency 2285 Hz. We can deduce that, a maximum power of 12.46W is obtained in this case for and load resistance R=1258.9 Ω. Figure 3(b) shows the profiles of the average power (solid curves) and the output voltage (dashed curves) as function of the load resistance R at the cavity mode frequency and

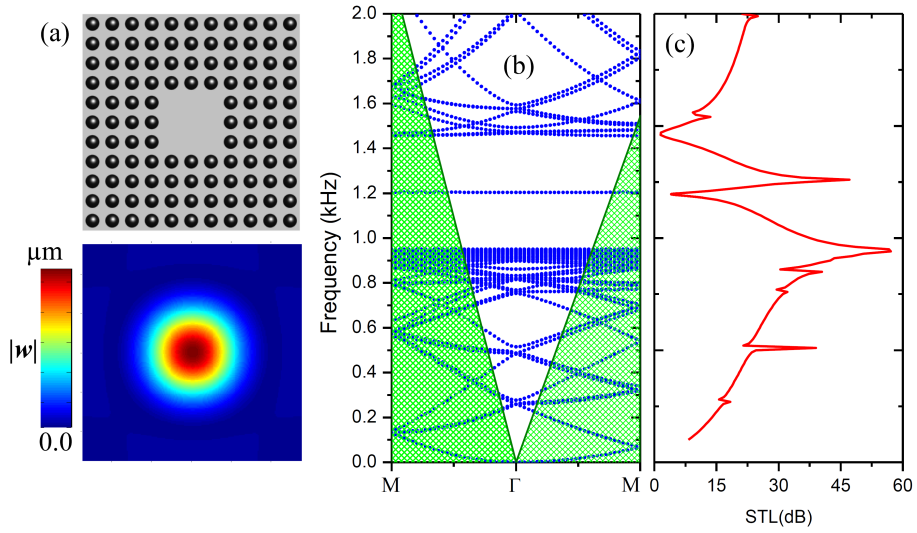

Figure 4. (a) Supercell of the AM Plate structure where the defect is created by removing the nine central resonators. (b) The band structure calculation for the supercell. (c) STL for loss factor $\eta = 0.005$. (d) The displacement field of the plate at the cavity mode frequency.

for PZT radius of 11.5 mm. The calculation were performed for both $\eta = 0.01$ and $\eta = 0.005$. As expected, the voltage increases and stabilizes at a constant value starting from $R = 10$ kΩ, and the electrical power is maximum at the optimized load resistance. The table in figure 3 summarizes the obtained results for maximum power output. One can see that the collected power is 12.46 μW for $\eta = 0.005$, and decreases to 4.35 for $\eta = 0.01$ because of the energy loss by the viscoelastic effect in the resonators. In the following studies we will consider the loss factor $\eta = 0.005$ for all the resonators.

The second system considered in this study is presented in figure 4(a) where the closest nine resonators from the center of the supercell are removed. In this system, in order to get a cavity mode which has the displacement field profile close to the one of the first system (figure 4(d)), the resonance frequency of the resonators is chosen to be 950 Hz. This choice will not only lower the band gap frequency edges to 950 Hz and 1456 Hz, but also make the cavity mode frequency located in the middle of the gap for the purpose of increasing the elastic energy confinement inside the created defect. figures 4(b) and 4(c) present the band structure as well as the STL for the system. The cavity mode is located at 1.2 kHz and the corresponding STL dip (high acoustic transmission) is at 4.04 dB which is much lower than the previous cavity system case (9.84 dB). Furthermore, we plot in figure 4(d) the displacement field profile of the cavity mode where the maximum of the vibration amplitude is 3 μm which is higher than the value found for the first structure (see table in figure 2). This is expected as the elastic vibration amplitude of the cavity mode is directly linked to the acoustic transmission of the acoustic wave. We expect then to harvest more energy in this case compared to the case of the first structure. figure 5presents the output power and

the voltage calculations for the system of figure 4(a) at the resonance frequency of the cavity mode. In this case, with the optimized load resistance R=1258.9 Ω and PZT radius of 16 mm, a maximum power of 15μW is obtained.

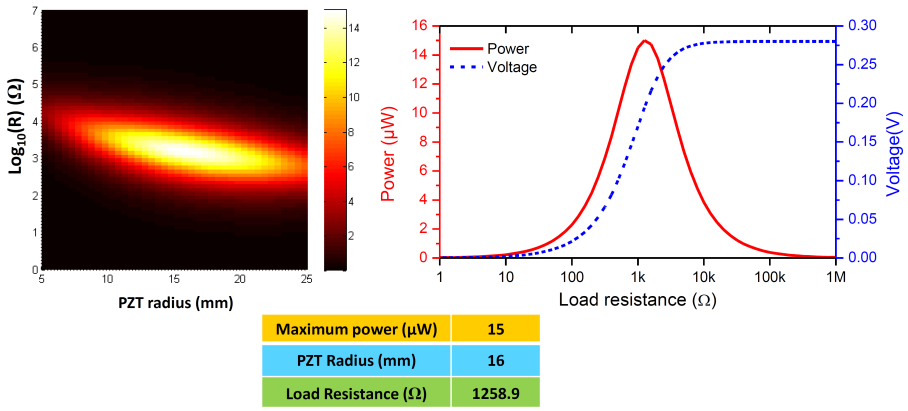

Maximum power (μW)	15
PZT Radius (mm)	16
Load Resistance (Ω)	1258.9

Figure 5. (Left) Output average power in color map as function of the PZT radius and the load resistance for =0.005 at the cavity mode frequency 1.2kHz. (Right) Out-put power (solid line) and voltage (dashed line) for PZT radius 16mm. The table summarizes the maximum power harvested with the optimal PZT radius and load resistance.

From these results, it becomes clear that the defect created by removing 9 resonators allows not only collecting more acoustic energy than the case of removing 5 resonators, but also open the possibility to reach a lower frequency as the AEH is performed at 1.2 kHz where the wavelength is larger than in the case of the first cavity (2.2 kHz). This can be understood by the fact that removing more resonators will offer more space to this kind of zero-order cavity mode to shape itself into the space defect at a specific wavelength in some way proportional to the defect space created. Thus, if we plan to lower the frequency to 500 Hz for example for the purpose of AEH, the wavelength of the flexural wave become larger so that we need to remove even more resonators to create enough space for the cavity mode to be created. This solution is unwelcome because of the necessity of large AM structure, not to mention the PZT patch dimension which will also be needed to be increased for maximum mechanical-to-electrical energy conversion. To overcome this limitation we propose another kind of defect in which we change the properties of the central resonators instead of removing them.

3.2. Small size defect system

In order to create a band gap in the frequency region around 500 Hz, we fix the resonant frequency of the resonators into $f_R = 400$Hz and their mass to $m_R = 368\ \mu$ g. The band gap

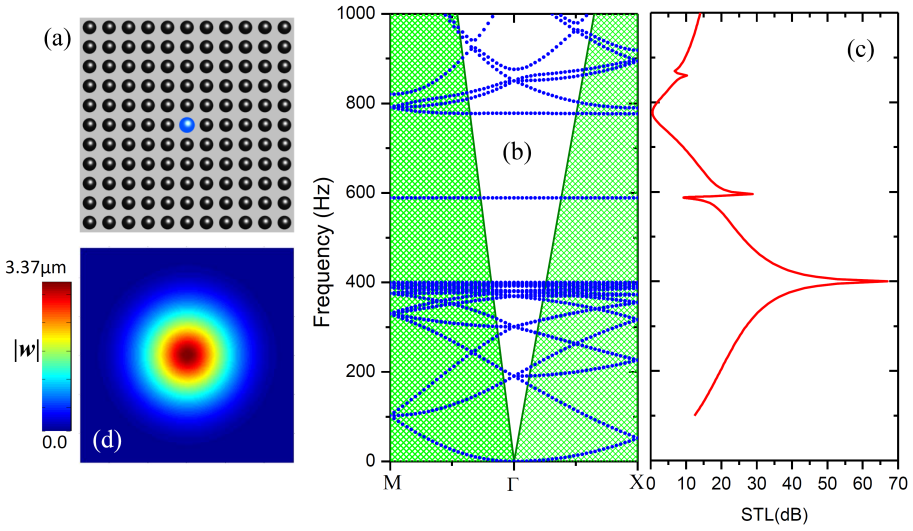

Figure 6. (a) Supercell of the AM Plate structure where the defect is created by changing the mechanical properties of the central resonator indicated by blue color. (b) The band structure calculation for the supercell. (c) STL for loss factor =0.005. (d) The displacement field of the plate at the cavity mode frequency.

lower and upper edges will be then 400 Hz and 771 Hz. In this section, we will study AEH by three super-cell systems having different type of defects introduced in the center. The first one is made of 11×11 unit cells in which we change the properties of the central resonator indicated by blue color in figure 6(a). The mass of the central resonator is kept the same as the other resonators while its resonance frequency is fixed to $f'_{\mathrm{R}} = 640\mathrm{Hz}$. This choice is based on putting the cavity modes frequency in the middle of the new band gap.

The band structure in figure 6(b) shows the cavity mode created in the middle of the band gap at 589Hz and the corresponding STL dip at 12.66 dB (figure 6(c)). figure 6(d) shows the out-of-plane displacement field of the plate at the cavity mode frequency. It can be deduced that the shape of the wave field is similar to the one of the previous cases where the defect is created by removing the resonators. Regarding the acoustic energy that can be harvested by the system where the PZT patch can be fixed at the center of the super-cells plate surface containing no resonators, figure 7 summarizes the results for the output power and voltage calculations.

In this case, the maximum power is 3.45 μW at the cavity mode frequency 589 Hz for the optimized load resistance of 6309.9 Ω and PZT radius of 10 mm. This value of the power is much lower than the previous cases. To increase the collected power, we thought about increasing the inertia of the cavity by increasing the mass of the central resonator to 736 μg which is twice the mass of the surrounding resonators, and at the same time we adjust the resonance frequency of the central resonator to $f'_{\mathrm{R}} = 700\mathrm{Hz}$ so as to have the cavity mode in the middle of the bad gap at exactly the same frequency 589 Hz. Figure 8 shows the obtained

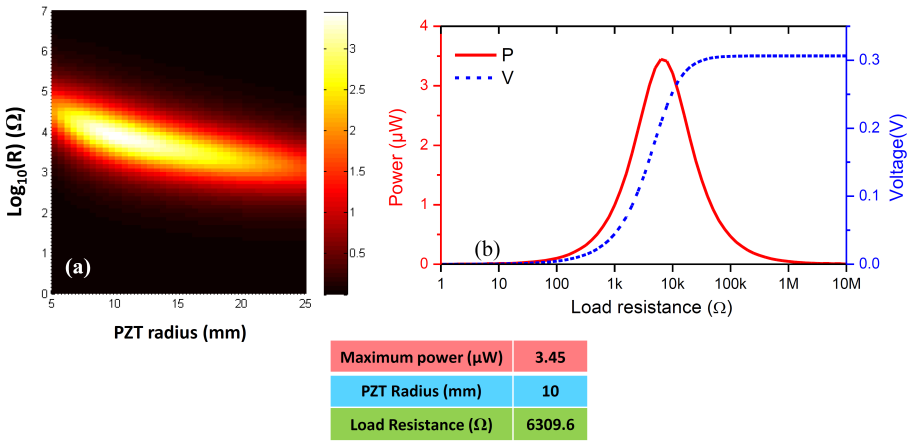

Figure 7. (a) Output average power in color map as function of the PZT radius and the load resistance for $\eta = 0.005$ at the cavity mode frequency 589 Hz. (b) Out-put power (solid line) and voltage (dashed line) for PZT radius 10 mm. The table summarizes the maximum power harvested with the optimal PZT radius and load resistance.

results for the output power and the voltage at the cavity mode frequency, i.e. 589 Hz, for an optimized PZT patch radius of 9.5 mm. The maximum power obtained is 7.54 μW for 7943.3 Ω which is higher than the previous case of figure 7. It is convincing that increasing the mass of the central resonator will introduce more inertia to the system in the center so that the amplitude of the out-of-plane displacement of the plate will be increased as well. This aspect can be deduced when comparing the wave field amplitude in figures 6 and 8.

Although these results are of interest, the power collected remains limited and one cannot indefinitely increase the mass of the central resonator especially when considering the lightweight criterion for the system. To increase the harvested power without changing the masses of the resonators, we chose to change the resonance frequency (i.e. the stiffness) of multiple resonators close to the super-cell center. We fix the masses of all the resonators in the super-cell to have the same value of 368 μg. We propose two systems presented in figures 9 and 10 in which the resonators indicated in blue have their resonance frequency changed. For the case of figure 9(a), the stiffness of the 5 central resonators is changed so that the resonance frequency is fixed to $f_R' = 1.5$kHz. This allows the creation of a cavity mode in the middle of the band gap at 589Hz. The displacement field profile of the mode plotted in figure 9(b) is similar to the one of the previous cases. Furthermore, as we can see in figure 9(c), the maximum power harvested in this case is 12.7 μW for 2511.9 Ω and 16mm for the PTZ radius. This value of the electrical power is in the same order of the power we got in the case of removing the 5 central resonators where the cavity mode is created at 2285 Hz (see figures 2 and 3). Thus, the main advantage of changing the resonators mechanical

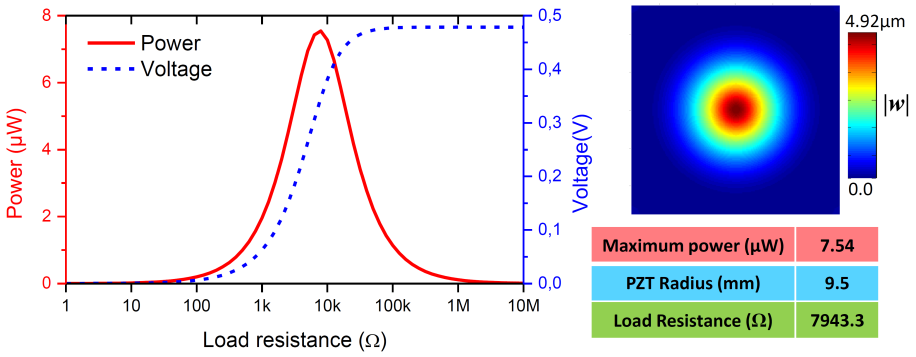

Figure 8. (Left) Out-put power (solid line) and voltage (dashed line) for PZT radius 9.5 mm at the cavity mode frequency 589 Hz. (Right) Displacement field of the plate at the cavity mode frequency. The table summarizes the maximum power harvested with the optimal PZT radius and load resistance.

properties is the possibility to control the frequency of the created cavity mode and be able to tune lower it down to 500 Hz, which is not the case of removing the resonators.

We pushed further our investigation by considering the system presented in figure 10 where the stiffness of 9 closest resonators to the super-cells center (indicated by blue in figure 10(a)) is considered to be infinite. Its like we consider the springs are rigid and only the mass effect on the plate is considered for these resonators. In this case, the cavity mode is found at 519 Hz and its wave displacement field shape is similar to the one of the previous cases as we can see in figure 10(b). For AEH, the calculations show that this kind of mode allows reaching a maximum power of 18.1 μW (see figure 10(c)) which is higher than the case of removing the 9 central resonators (figures 4 and 5). Furthermore, in the case of open cavity presented in figure 4, at the frequency 1.2 kHz, the wavelength is 28.3 cm in air and 6.38 cm for the flexural wave of the bare plate (without resonator) which is in the same order of the defect size. However, in the case of figure 10, the wavelength is larger at 519 Hz: 65.5 cm in air and 9.7 cm for the flexural wave of the bare plate while the defect size introduced in the supercell is the same as the one of the case of open cavity of figure 4. One can then deduce the sub-wavelength functionality of the designed cavity for the purpose of AEH. Regarding the energy density, its evaluation depends on the resonators design and space occupation and cannot be evaluated precisely in this study since we only consider their force applied to the plate surface in the analytical model. If we consider resonators with a pillar design having the same dimension considered in our previous work [23], the expected energy density provided by the system would almost be 0.78 μW/cm^3 which is higher than what was produced by

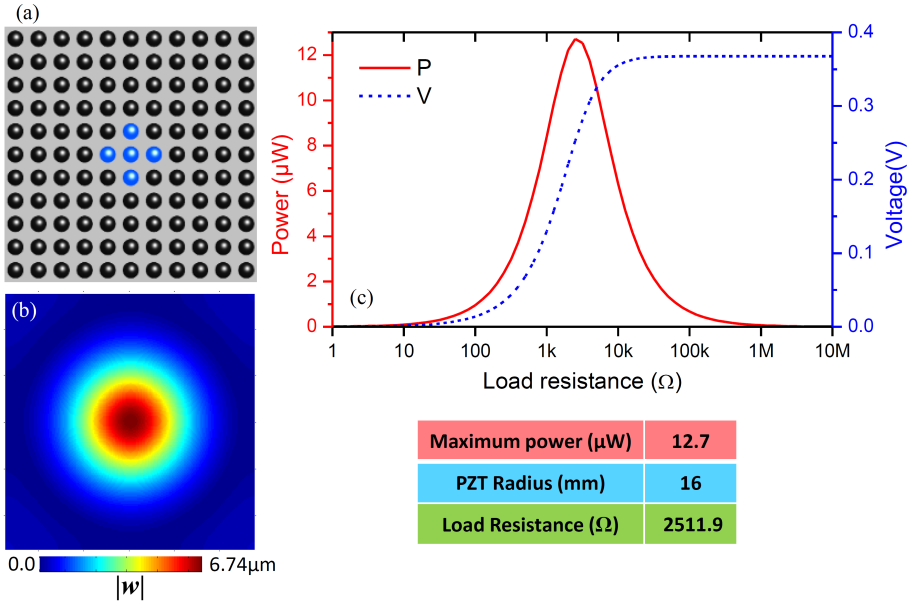

Figure 9. (a) Supercell of the AM plate structure where the defect is created by changing the stiffness of the 5 central resonators indicated by blue color. (b) Displacement field of the plate at the cavity mode frequency. (c) Output power (solid line) and voltage (dashed line) for PZT radius 16mm at the cavity mode frequency 589 Hz. The table summarizes the maximum power harvested with the optimal PZT radius and load resistance.

sonic crystals (0.14 μW/cm^3) [14] or Helmholtz resonator based system (μW/cm^3) [3].

Furthermore, in the case of open cavity presented in Fig. 4, at the frequency 1.2 kHz, the wavelength is 28.3 cm in air and 6.38 cm for the flexural wave of the bare plate (without resonator) which is in the same order of the defect size. However, in the case of Fig. 10, the wavelength is larger at 519 Hz: 65.5 cm in air and 9.7 cm for the flexural wave of the bare plate while the defect size introduced in the supercell is the same as the one of the case of open cavity of Fig. 4. One can then deduce the sub-wavelength functionality of the designed cavity for the purpose of AEH.

From these studies, it is clear that the stiffness and the mass of the resonators are of great importance for the design of such structure. In practical point of view, one kind of resonator that can be proposed is a composite pillar made of rigid mass over a low stiffness material such as rubber [11, 37]. The materials and the geometry of the pillars must be chosen carefully to insure a good mechanical response.

4. Conclusion

In summary, we developed a feasible yet high effective analytical method to describe the AEH with an AM plate. By taking advantage of AM special acoustic properties, we proposed a simple way of introducing a small size defect to achieve sub-wavelength acoustic energy confinement for the purpose of AEH. With a sub-wavelength cavity mode located at 519

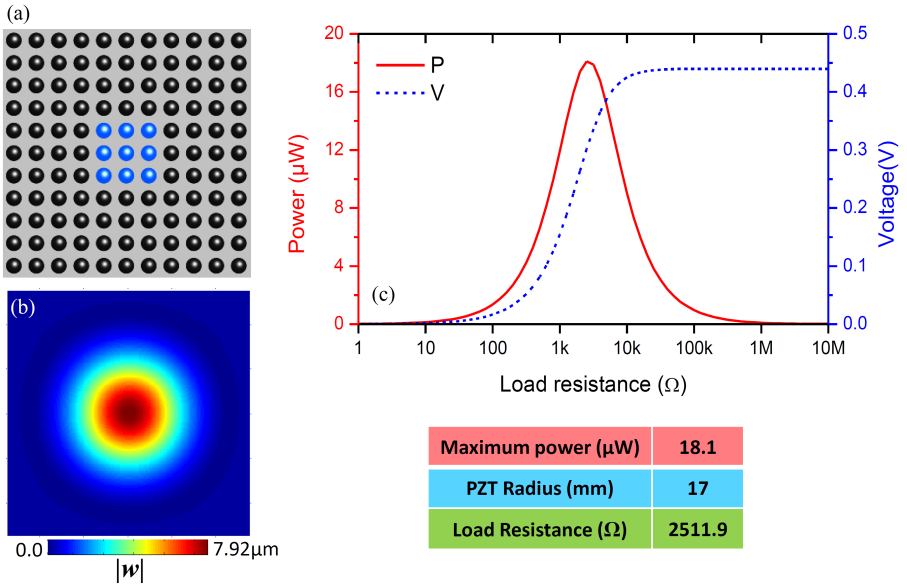

Figure 10. (a) Supercell of the AM plate structure where the defect is created by changing the stiffness of 9 central resonators indicated by blue color. (b) Displacement field of the plate at the cavity mode frequency. (c) Output power (solid line) and voltage (dashed line) for PZT radius 16mm at the cavity mode frequency 519 Hz. The table summarizes the maximum power harvested with the optimal PZT radius and load resistance.

Hz, we were able to harvest 18.1 μW of acoustic energy for an incident plate wave of 100 dB SPL. The frequency of the cavity mode can be easily tuned by changing the properties of the resonators. It is noteworthy pointing out that the analytical model doesnt take into account the mass and stiffness effects of the PZT. To analyze this aspect, we performed a FEM simulation based on the model developed for our recent work [23] where the stiffness and the mass of the circular PTZ patch are considered as well as the electromechanical coupling. The simulation was done for the last system presented in the work. We found out that the defect mode frequency is located at 530 Hz where a maximum power of 2 μW is collected. Comparing these results with the ones provided by the analytical model, the shift of the defect frequency is expected as it will be lower if the stiffness of the PZT is not considered. Furthermore, the power collected value of 22 μW is higher than the one estimated by the analytical model because of the cavity inertia which is higher when considering the mass of the PZT. Although the analytical and FEM results are slightly different, the analytical model offers good estimation of the collected power because of the small thickness of the PZT. The idea here is to present a simple analytical model to estimate the energy that can be harvested from the mechanical strain introduced by the cavity mode inside the created defect in the AM super-cell. The results are obtained in few minutes compared to FEM which is time consuming when applied to this kind of system.

Acknowledgments

This work was supported by the startup grant at Tongji University.
MO acknowledge support for this work from University of Lorraine

References

[1] S. B. Horowitz, M. Sheplak, L. N. Cattafesta, and T. Nishida. A mems acoustic energy harvester. *J. Micromech. Microeng.*, 16:S174, 2006.

[2] S. Noh, H. Lee, and B. Choi. A study on the acoustic energy harvesting with helmholtz resonator and piezoelectric cantilevers. *Int. J. Precis. Eng. Manuf.*, 14:1629, 2013.

[3] B. Li, A. J. Laviage, J. H. You, and Y. J. Kim. Harvesting low-frequency acoustic energy using quarter-wavelength straight-tube acoustic resonator. *Appl. Acoust.*, 74:1271, 2013.

[4] B. Li, J. H. You, and Y. J. Kim. Low frequency acoustic energy harvesting using pzt piezoelectric plates in a straight tube resonator. *Smart Mater. Struct.*, 22:055013, 2013.

[5] M. S. Kushwaha, P. Halevi, L. Dobrzynski, and B. Djafari-Rouhani. Acoustic band structure of periodic elastic composites. *Phys. Rev. Lett.*, 71:2022, 1993.

[6] M. Sigalas and E. N. Economou. Band structure of elastic waves in two dimensional systems. *Solid State Commun.*, 86:141, 1993.

[7] Y. Chen and L. Wang. Periodic co-continuous acoustic metamaterials with overlapping locally resonant and bragg band gaps. *Appl. Phys. Lett.*, 105:191907, 2014.

[8] Y. Chen and L. Wang. Multiband wave filtering and waveguiding in bio-inspired hierarchical composites. *Extreme Mech. Lett.*, 5:18, 2015.

[9] M. M. Sigalas. Defect states of acoustic waves in a two-dimensional lattice of solid cylinders. *J. Appl. Phys.*, 84:3026, 1998.

[10] S. El-Jallal, M. Oudich, Y. Pennec, B. Djafari-Rouhani, A. Makhoute, Q. Rolland, S. Dupont, and J. Gazalet. Optomechanical interactions in two-dimensional si and gaas phoxonic cavities. *J. Phys. Condens. Matter*, 26:015005, 2014.

[11] M. Oudich, Y. Li, B. M. Assouar, and Z. Hou. A sonic band gap based on the locally resonant phononic plates with stubs. *New J. Phys.*, 12:083049, 2010.

[12] L. Y. Wu, L. W. Chen, and C. M. Liu. Acoustic energy harvesting using resonant cavity of a sonic crystal. *Appl. Phys. Lett.*, 95:013506, 2009.

[13] W. C. Wang, L. Y. Wu, L. W. Chen, and C. M. Liu. Acoustic energy harvesting by piezoelectric curved beams in the cavity of a sonic crystal. *Smart Materials & Structures*, 19:045016, 2010.

[14] A. Yang, P. Li, Y. Wen, C. Lu, X. Peng, J. Zhang, and W. He. Enhanced acoustic energy harvesting using coupled resonance structure of sonic crystal and helmholtz resonator. *Appl. Phys. Express*, 6:127101, 2013.

[15] Z. Liu, X. Zhang, Y. Mao, Y. Y. Zhu, Z. Yang, C. T. Chan, and P. Sheng. Locally resonant sonic materials. *Science*, 289:1734, 2000.

[16] B. Assouar, M. Oudich, and X. Zhou. Acoustic metamaterials for sound mitigation. *C. R. Physique*, 17:524, 2016.

[17] N. Fang, D. Xi, J. Xu, M. Ambati, W. Srituravanich, C. Sun, and X. Zhang. Ultrasonic metamaterials with negative modulus. *Nat. Mater.*, 5:452, 2006.

[18] Y. Ding, Z. Liu, C. Qiu, and J. Shi. Metamaterial with simultaneously negative bulk modulus and mass density. *Phys. Rev. Lett.*, 99:093904, 2007.

[19] Z. Yang, J. Mei, M. Yang, N. H. Chan, and P. Sheng. Membrane-type acoustic metamaterial with negative dynamic mass. *Phys. Rev. Lett.*, 101:204301, 2008.

[20] B. Liang, B. Yuan, and J. C. Cheng. Acoustic diode: rectification of acoustic energy flux in one-dimensional systems. *Phys. Rev. Lett.*, 103:104301, 2009.

[21] B. Liang, X. S. Guo, J. Tu, D. Zhang, and J. C. Cheng. An acoustic rectifier. *Nat. Mater.*, 9:989, 2010.

[22] Z. Liang and J. Li. Extreme acoustic metamaterial by coiling up space. *Phys. Rev. Lett.*, 108:114301, 2012.

[23] S. Qi, M. Oudich, Y. Li, and B. Assouar. Acoustic energy harvesting based on a planar acoustic metamaterial. *Appl. Phys. Lett.*, 108:263501, 2016.

[24] M. Oudich, B. Djafari-Rouhani, Y. Pennec, M. B. Assouar, and B. Bonello. Negative effective mass density of acoustic metamaterial plate decorated with low frequency resonant pillars. *J. Appl. Phys.*, 116:184504, 2014.

[25] C. Shen, J. Xu, N. X. Fang, and Y. Jing. Anisotropic complementary acoustic metamaterial for canceling out aberrating layers. *Phys. Rev. X*, 4:041033, 2014.

[26] C. Shen, Y. Xie, N. Sui, W. Wang, S. A. Cummer, and Y. Jing. Broadband acoustic hyperbolic metamaterial. *Phys. Rev. Lett.*, 115:254301, 2015.

[27] G. Ma and P. Sheng. Acoustic metamaterials: From local resonances to broad horizons. *Sci. Adv.*, 2:e1501595, 2016.

[28] S. A. Cummer, J. Christensen, and A. Alu. Controlling sound with acoustic metamaterials. *Nat. Rev. Mat.*, 1:16001, 2016.

[29] Y. Li, B. Liang, Z. M. Gu, X. Y. Zou, and J. C. Cheng. Reflected wavefront manipulation based on ultrathin planar acoustic metasurfaces. *Sci. Rep.*, 3:2546, 2013.

[30] Y. Li, X. Jiang, R. Q. Li, B. Liang, X. Y. Zou, L. L. Yin, and J. C. Cheng. Experimental realization of full control of reflected waves with subwavelength acoustic metasurfaces. *Phys. Rev. Applied*, 2:064002, 2014.

[31] Y. Li, X. Jiang, B. Liang, J. C. Cheng, and L. K. Zhang. Metascreen-based acoustic passive phased array. *Phys. Rev. Applied*, 4:024003, 2015.

[32] J. Mei, G. Ma, M. Yang, Z. Yang, W. Wen, and P. Sheng. Dark acoustic metamaterials as super absorbers for low-frequency sound. *Nat. Commun.*, 3:756, 2012.

[33] G. Ma, M. Yang, S. Xiao, Z. Yang, and P. Sheng. Acoustic metasurface with hybrid resonances. *Nat. Mater.*, 13:873, 2014.

[34] K. M. Ho, Z. Yang, X. X. Zhang, and P. Sheng. Measurements of sound transmission through panels of locally resonant materials between impedance tubes. *Appl. Acoust.*, 66:751, 2005.

[35] Y. Xiao, J. Wen, and X. Wen. Sound transmission loss of metamaterial-based thin plates with multiple subwavelength arrays of attached resonators. *J. Sound Vib.*, 331:5408, 2012.

[36] M. Oudich, X. M. Zhou, and M. B. Assouar. General analytical approach for sound transmission loss analysis through a thick metamaterial plate. *J. Appl. Phys.*, 116:193509, 2014.

[37] B. M. Assouar, M. Senesi, M. Oudich, M. Ruzzene, and Z. Hou. Broadband plate-type acoustic metamaterial for low-frequency sound attenuation. *Appl. Phys. Lett.*, 101:173505, 2012.